Proceedings of IDETC/CIE 2012
ASME 2012 International Design Engineering Technical Conferences & Computers and Information in Engineering Conference
August 12 - 15, 2012, Chicago, Illinois, USA

DETC2012-70277

MECHANISM BRANCHES, TURNING CURVES, AND CRITICAL POINTS

David H. Myszka
University of Dayton
Dayton, Ohio 45469
Email: dmyszka1@udayton.edu

Andrew P. Murray
University of Dayton
Dayton, Ohio 45469
Email: amurray1@udayton.edu

Charles W. Wampler
General Motors R&D Center
Warren, Michigan 48090
Email: charles.w.wampler@gm.com

ABSTRACT

This paper considers single-degree-of-freedom, closed-loop linkages with a designated input angle and one design parameter. For a fixed value of the design parameter, a linkage has *turning points* (dead-input singularities), which break the motion curve into branches such that the motion along each branch can be driven monotonically from the input. As the design parameter changes, the number of branches and their connections, in short the topology of the motion curve, may change at certain *critical points*. As the design parameter changes, the turning points sweep out a curve we call the "turning curve," and the critical points are the singularities in this curve with respect to the design parameter. The critical points have succinct geometric interpretations as transition linkages. We present a general method to compute the turning curve and its critical points. As an example, the method is used on a Stephenson II linkage. Additionally, the Stephenson III linkage is revisited where the input angle is able to rotate more than one revolution between singularities. This characteristic is associated with cusps on the turning point curve.

1 Introduction

Direct (or forward) kinematic position analysis of a single degree-of-freedom (dof) linkage involves determining values for joint parameters for a given position of the input link. Since the governing kinematic constraint equations for the links in a closed-loop linkage are non-linear, multiple solutions are obtained for a single position of the input link. Erdman, et. al., [1] refer to each solution as a ***geometric inversion*** (GI) and is associated with an alternate configuration of the mechanism at the specific input. The traditional solution method for a direct kinematic problem is completed by using tangent-half-angle substitutions for the output variables [2]. More efficiently, Wampler [3, 4] presents techniques for using isotropic coordinates to generate polynomial equations that describe the position of a general single-dof linkage. Solution of the complex, polynomial systems can be readily accomplished by using numerical polynomial continuation [6]. The set of position equations is represented by a ***motion curve***, which exhibits the relationships between the joint variables and whose trace is created by plotting the GIs for various positions of the input link. The trace of the motion curve projected onto two dimensions (one being the input variable) is often referred to as input-output plots [1]. These traces for even common linkages can be quite convoluted involving multiple segments.

A ***circuit*** of a mechanism is defined by Chase and Mirth [7] as the set of all possible orientations of links that can be realized without disconnecting any of the joints. If a mechanism must be disassembled to move from one position to another, the two positions reside on separate circuits. Foster and Cipra [8, 9] use the term assembly configuration to refer to a circuit. Each segment on the trace of the motion curve represents a different circuit. At a specific input link position, each GI may lie on a different circuit, but several GIs can lie on the same circuit. The circuits of a mechanism are independent of the choice of driving link, and there is no direct relationship between the geometric inversions and circuits [7]. Established methods to identify different circuits rely on geometric insights of a particular mechanism [8–13].

Singularity points exist when the driving link is no longer

able to move the mechanism. At the singularity points, also called stationary points or more vividly dead-input points, the mechanism becomes locked and the mechanical advantage reduces to zero [14, 15]. On the trace of the motion curve, the linkage singularities appear as turning points, and are referred to as ***turning points*** in this paper. Turning points of a mechanism are dependent on the choice of driving link and must be avoided when attempting to smoothly operate the mechanism. Chase and Mirth [7] defined the regions on a circuit between turning points as ***branches***. For single-dof linkages, turning points are the input limits for that branch. If a GI resides on a motion curve segment (i.e., circuit) that has no singularities, it can be driven with a fully rotatable crank.

A ***turning point plot*** is the trace of turning points with respect to the input angle and a designated design parameter. Observing the motion characteristics as a design parameter is considered a variable provides insight into the design space for a particular linkage. Further, understanding the motion regime limits with respect to a design parameter can assist the synthesis process of adjustable linkages, as in [16, 17]. Myszka et. al. [18] extend the work of Wenger et. al. [19, 20] and apply a turning point plot to single-dof linkages to distinguish zones of identical GIs. Myszka et. al. observed that local extrema on the turning curve, termed ***critical points***, correspond to a change in the number of circuits.

Murray et al. [21] use the transition linkage concept to classify single-dof linkages. Transition linkages contain link lengths that lie on the boundary of physically realizable linkages or between linkages with distinct motion characteristics. Myszka, et. al., also observe that the critical points on the turning curve plot correspond with transition linkages. However, the method used in [18] to create a turning point curve is computationally intensive and impractical for multi-loop linkages. Wampler's method of using isotropic coordinates to represent mechanism links facilitates the solution of kinematic equations. This paper implements isotropic coordinates to provide a general method to accurately compute the motion curves, turning curve and critical points for any linkage.

2 Isotropic Coordinates

In kinematic formulations, it is common to consider links to be vectors in the complex plane [1]. A unit vector defined by θ_j and shown in Fig 1 can be represented in polar form as,

$$\mathbf{T}_j = e^{i\theta_j}. \tag{1}$$

where $i = \sqrt{-1}$. Subsequently, a binary mechanism link is represented as $a_j\mathbf{T}_j$, where $a_j \in \mathbb{R}$ is the length of the link. Applying

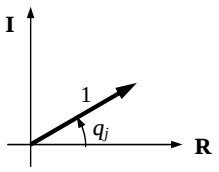

Figure 1: A unit vector plotted on the complex plane.

the Euler identity, the components of the unit vector are

$$\mathbf{T}_j = \cos\theta_j + i\sin\theta_j. \tag{2}$$

The complex conjugate of $\mathbf{T}_j$ is

$$\overline{\mathbf{T}}_j = e^{-i\theta_j} = \cos\theta_j - i\sin\theta_j, \tag{3}$$

and

$$\mathbf{T}_j\overline{\mathbf{T}}_j = e^{i\theta_j}e^{-i\theta_j} = 1. \tag{4}$$

Mechanism links that are represented by exponential variables and their conjugates are isotropic coordinates. A more complete discussion of isotropic coordinates and their properties can be found in Wampler [5].

It is important to note that when working in isotropic coordinates the terms "real solution" or "real point" take on an unusual meaning. When we solve a polynomial system whose variables include $\mathbf{T}_j$ or $\overline{\mathbf{T}}_j$, "real" is taken to mean that the corresponding angle θ_j is real. This implies that $|\mathbf{T}_j| = |\overline{\mathbf{T}}_j| = 1$.

The partial derivatives of $\mathbf{T}_j$ and $\overline{\mathbf{T}}_j$ are

$$\left(\frac{\partial}{\partial\theta_j}\right)\mathbf{T}_j = i\mathbf{T}_j, \qquad \left(\frac{\partial}{\partial\theta_j}\right)\overline{\mathbf{T}}_j = -i\overline{\mathbf{T}}_j \tag{5}$$

The geometric interpretation of some of the formulas to follow is aided by the following lemma.

Lemma 2.1. *Let* $\mathbf{A}$ *and* $\mathbf{B}$ *be nonzero complex vectors. Then the condition*

$$\mathbf{A}\bar{\mathbf{B}} - \bar{\mathbf{A}}\mathbf{B} = 0$$

implies that $\mathbf{A}$ *and* $\mathbf{B}$ *are parallel.*

Proof. Multiply through by $\mathbf{AB}$ to obtain

$$\mathbf{A}^2\mathbf{B}\bar{\mathbf{B}} - \mathbf{A}\bar{\mathbf{A}}\mathbf{B}^2 = 0.$$

Applying (4), $\mathbf{A}\bar{\mathbf{A}} = a^2$ and $\mathbf{B}\bar{\mathbf{B}} = b^2$, where a and b are the lengths of $\mathbf{A}$ and $\mathbf{B}$, respectively. So the expression factors as

$$(b\mathbf{A} + a\mathbf{B})(b\mathbf{A} - a\mathbf{B}) = 0.$$

which requires either $(b\mathbf{A} + a\mathbf{B}) = 0$ or $(b\mathbf{A} - a\mathbf{B}) = 0$. If $(b\mathbf{A} + a\mathbf{B}) = 0$ then $\mathbf{A}$ and $\mathbf{B}$ are in opposite directions. If $(b\mathbf{A} - a\mathbf{B}) = 0$ then $\mathbf{A}$ and $\mathbf{B}$ are in the same direction. In either case, $\mathbf{A}$ and $\mathbf{B}$ are parallel.

3 Turning Points, Turning Curve, and Critical Points

In this section, we present our general methodology, using the most basic closed-chain mechanism, the four-bar linkage, for illustration. In the following sections, we will apply the method to the more challenging cases of the Stephenson II and Stephenson III linkages.

Consider a general mechanism with a single dof. The input variable is designated as $x \in \mathbb{C}$. Also, designate a design variable, $p \in \mathbb{C}$, and let y be all the remaining variables $y \in \mathbb{C}^N$. We assume that the loop closure equations are formulated as

$$f(p,x,y) = 0, \qquad f : \mathbb{C} \times \mathbb{C} \times \mathbb{C}^N \to \mathbb{C}^N. \tag{6}$$

For a fixed value of p, the mechanism has a single dof motion represented by a motion curve $\mathcal{C}_p \subset \mathbb{C}^{N+1}$, $\dim(\mathcal{C}_p) = 1$.

Example 3.1. [Four-bar loop equations] There are various choices for formulating loop closure equations and we shall make use of two closely related ones, both of which model links as vectors in the complex plane. As an illustration, consider the four-bar linkage as shown in Fig. 2. Designate the input as angle $x = \theta_2$ and the design parameter as $p = a_4$. The remaining variables are $y = \{\theta_3, \theta_4\}$, while θ_1 and a_1, a_2, a_3 are taken as given. The four-bar has a single loop, whose closure condition in complex exponential notation is given as

$$f = a_1 e^{i\theta_1} + a_2 e^{i\theta_2} + a_3 e^{i\theta_3} + a_4 e^{i\theta_4} = 0. \tag{7}$$

With a_4 fixed, the real and imaginary parts of this complex equation impose two constraints on $\{\theta_2, \theta_3, \theta_4\}$, resulting in a motion curve as illustrated in Fig. 3.

An alternative to the exponential form is to convert (7) to its equivalent isotropic form as

$$\begin{aligned} g &= a_1\mathbf{T}_1 + a_2\mathbf{T}_2 + a_3\mathbf{T}_3 + a_4\mathbf{T}_4 = 0, \\ \bar{g} &= a_1\overline{\mathbf{T}}_1 + a_2\overline{\mathbf{T}}_2 + a_3\overline{\mathbf{T}}_3 + a_4\overline{\mathbf{T}}_4 = 0, \\ h_2 &= \mathbf{T}_2\overline{\mathbf{T}}_2 - 1 = 0, \\ h_3 &= \mathbf{T}_3\overline{\mathbf{T}}_3 - 1 = 0, \\ h_4 &= \mathbf{T}_4\overline{\mathbf{T}}_4 - 1 = 0. \end{aligned} \tag{8}$$

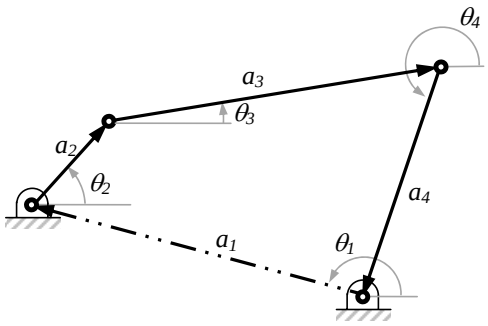

Figure 2: A four-bar mechanism.

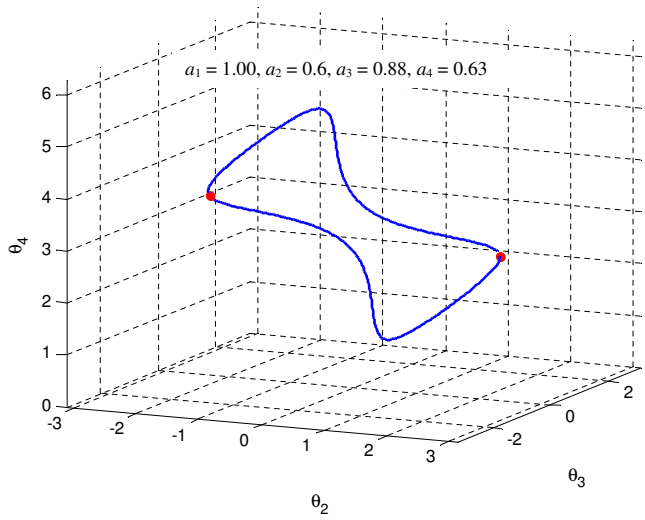

Figure 3: The motion curve for a four-bar mechanism as expressed in Eq. 7 or 8.

With a_4 fixed, this system of five equations describes a curve in the six-dimensional space of $\{\mathbf{T}_2, \mathbf{T}_3, \mathbf{T}_4, \overline{\mathbf{T}}_2, \overline{\mathbf{T}}_3, \overline{\mathbf{T}}_4\}$. The points of this curve are in one-to-one correspondence with the points of the curve described by (7), and we may think of them as the same four-bar motion curve. The isotropic formulation has the convenient property that all its equations are polynomial, which facilitates finding solutions, while the complex exponential formulation is more compact. We will move fluidly between the two approaches as convenient below.

The exponential form of the loop closure conditions for any n-link ℓ-loop planar mechanism with rotational joints can be written as

$$f_k = \sum_{j=1}^{n} a_{jk} e^{i\theta_j} = 0, \qquad k = 1, \ldots, \ell. \tag{9}$$

The coefficient $a_{jk} \in \mathbb{C}$, is the edge of link j that connects joints in loop k. For a binary link, there is just one edge, and it can be taken as a real number, its length. Ternary links (triangles) and higher will have different edges participating in different loops and the associated coefficients are then complex. See [4] and Sec. 4.

The ℓ loop equations in the exponential form of (9) convert to $2\ell + n - 1$ equations in isotropic coordinates as:

$$g_k = \sum_{j=1}^{n} a_{jk}\mathbf{T}_j = 0, \qquad \bar{g}_k = \sum_{j=1}^{n} a'_{jk}\overline{\mathbf{T}}_j = 0, \qquad k = 1,\ldots,\ell \tag{10}$$

$$h_j = \mathbf{T}_j\overline{\mathbf{T}}_j - 1 = 0, \qquad j = 2,\ldots,n. \tag{11}$$

Note that in the conjugate loop equations, $\bar{g}_k$, the complex conjugates, a'_{jk}, of the link edges appear. We do not include $\mathbf{T}_1\overline{\mathbf{T}}_1 - 1 = 0$ because link 1 is assumed to be the ground link and so its angle θ_1 is known.

3.1 Problem 1: Forward Kinematics

With the design parameter,p, fixed, the solution to (6) for a given input x is the direct kinematic problem and each solution is a GI. The isotropic formulation can be solved by any method applicable to systems of polynomial equations. However, before proceeding, it can be useful to reduce the basic formulation to a more compact form. First, since the input angle is given, the associated unit-length equation is dropped. In the case of the four-bar, where θ_2 is designated as the input, h_2 is dropped from (10). Next, the loop equations, g_k, and the conjugate loop equations, $\bar{g}_k$ are all linear, so these may be used to eliminate some variables. For example, for the four-bar of (8) the equations $g = 0$ and $\bar{g} = 0$ lead to defining the expressions

$$\begin{aligned} \mathbf{R}_4 &:= a_1\mathbf{T}_1 + a_2\mathbf{T}_2 + a_3\mathbf{T}_3, \\ \overline{\mathbf{R}}_4 &:= a_1\overline{\mathbf{T}}_1 + a_2\overline{\mathbf{T}}_2 + a_3\overline{\mathbf{T}}_3, \end{aligned} \tag{12}$$

so that $\mathbf{R}_4 = -a_4\mathbf{T}_4$ and $\overline{\mathbf{R}}_4 = -a_4\overline{\mathbf{T}}_4$. Accordingly, for $a_4 \neq 0$, we may form $a_4^2 h_4 = 0$ to get

$$H_4 := \mathbf{R}_4\overline{\mathbf{R}}_4 - a_4^2 = 0. \tag{13}$$

This equation along with $h_3 = \mathbf{T}_3\overline{\mathbf{T}}_3 - 1 = 0$ make a system of two equations for $\{\mathbf{T}_3, \overline{\mathbf{T}}_3\}$. This is the form of the equations that will be most useful later in the paper. These two polynomials can be solved many ways: one is to use $h_3 = 0$ to write $\overline{\mathbf{T}}_3 = 1/\mathbf{T}_3$, which after substitution into (13), gives a quadratic equation for $\mathbf{T}_3$.

In [3, 4], one can find recipes for solving general planar mechanisms formulated in isotropic coordinates as in (10). Similar to the derivation just discussed for the four-bar, the recipe in [3] eliminates half of the variables using the loop equations and then solves the system of bilinear polynomials using the Dixon determinant. (See [22] for a related method based on the Dixon determinant but using tangent-half-angle substitutions.)

3.2 Problem 2: Find all Turning Points

Given a mechanism (i.e., a fixed design parameter p), it is desirable to find all branches of the motion with respect to the designated input parameter, x. As illustrated in Figure 4 and described in [7], the branches meet at the *turning points* of the curve, where the mechanism moves differentially without any motion at the input. The mechanism is locked at a turning point (i.e., singular position), but can be driven smoothly from the input along each motion branch.

For fixed p, the tangent $[\Delta x, \Delta y]$ to the motion curve is given by

$$f_x\Delta x + f_y\Delta y = 0. \tag{14}$$

where $f_x = \frac{\partial f}{\partial x} \in \mathbb{C}^{N\times 1}$ and $f_y = \frac{\partial f}{\partial y} \in \mathbb{C}^{N\times N}$. The turning points occur when $\Delta y \neq 0$ with $\Delta x = 0$, which implies that

$$D(p,x,y) := \det f_y = 0. \tag{15}$$

Accordingly, the turning points are solutions to the system of equations

$$F(p,x,y) = \begin{bmatrix} f(p,x,y) \\ D(p,x,y) \end{bmatrix} = 0. \tag{16}$$

For given p, this is a system of $N+1$ equations in $N+1$ unknowns which can be solved to find the turning points. An alternative formulation that avoids forming the determinant is to solve for tangent vectors that have no x-component, that is, randomly choose a $1 \times N$ vector v and solve the system

$$\hat{F}(p,x,y,\Delta y) = \begin{bmatrix} f(p,x,y) \\ f_y\Delta y \\ v\cdot\Delta y - 1 \end{bmatrix} = 0. \tag{17}$$

Note that if Δy is a solution to $f_y\Delta y = 0$, then so is $\alpha\Delta y$ for any scalar α. The randomly chosen v picks out a unique scaling of the tangent vector.[1] The final expression ($v\,\Delta y - 1 = 0$) ensures

[1] This is equivalent to considering Δy as homogeneous coordinates on $\mathbb{P}^{N-1}$ and using v to choose a random patch on the representation of $\mathbb{P}^{N-1}$ [23, Chap. 3].

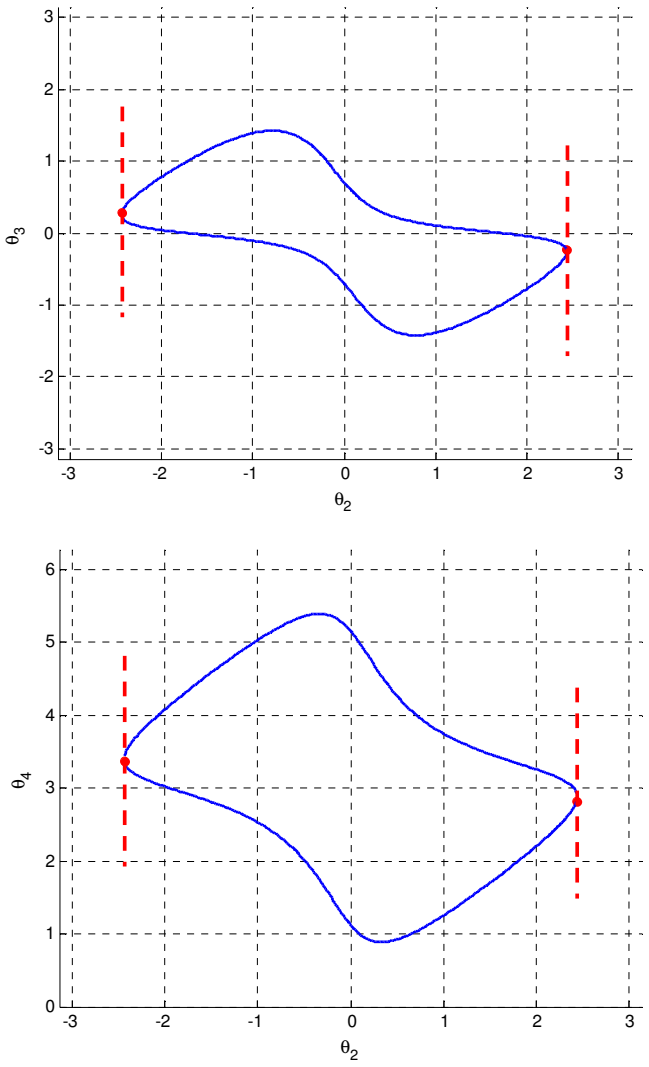

Figure 4: Projections of the motion curve from Fig. 3. Turning points, shown with red markers, have no x (θ_2 in this case) component.

$\Delta y \neq 0$. Since higher-dimensional tangent spaces are possible, one must search for these when solving (17). Methods for doing so are discussed in [23, Part II] and are available in the Bertini software package [25].

Let us return to the four-bar example to illustrate. The loop closure conditions are $\{h_2, h_3, H_4\} = 0$ from (8,13). Using (5), the partial derivatives of h_2 are

$$\frac{\partial h_2}{\partial \theta_2} = i\mathbf{T}_2\overline{\mathbf{T}}_2 - i\mathbf{T}_2\overline{\mathbf{T}}_2 \equiv 0, \quad \text{and} \quad \frac{\partial h_2}{\partial \theta_3} \equiv 0, \tag{18}$$

and similarly for h_3, so the only nontrival partial derivatives are those for H_4:

$$f_x = \frac{\partial f}{\partial \theta_2} = ia_2(\mathbf{T}_2\overline{\mathbf{R}}_4 - \mathbf{R}_4\overline{\mathbf{T}}_2), \tag{19}$$

$$f_y = \frac{\partial f}{\partial \theta_2} = ia_3(\mathbf{T}_3\overline{\mathbf{R}}_4 - \mathbf{R}_4\overline{\mathbf{T}}_3). \tag{20}$$

Since f_y is 1×1 in this instance, its determinant is itself. We may cancel the common factor of ia_3 and write the system that determines the turning points as

$$F = \begin{bmatrix} \mathbf{T}_2\overline{\mathbf{T}}_2 - 1 \\ \mathbf{T}_3\overline{\mathbf{T}}_3 - 1 \\ \mathbf{R}_4\overline{\mathbf{R}}_4 - a_4^2 \\ \mathbf{T}_3\overline{\mathbf{R}}_4 - \overline{\mathbf{T}}_3\mathbf{R}_4 \end{bmatrix} = 0. \tag{21}$$

This is a polynomial system of four equations in $\{\mathbf{T}_2, \mathbf{T}_3, \overline{\mathbf{T}}_2, \overline{\mathbf{T}}_3\}$. As a bilinear system in $\{\mathbf{T}_2, \mathbf{T}_3\}, \{\overline{\mathbf{T}}_2, \overline{\mathbf{T}}_3\}$, it has at most six solutions [23, Sec. 8.4.2], but it can be seen that two of these go to infinity, leaving just four finite roots.

By Lemma 2.1, we see that the turning point condition implies that links 3 and 4 are parallel. This is the well-known dead-input condition for a four-bar. With this geometric interpretation, one may find the turning points by solving first a triangle with sides $a_1, a_2, (a_3 + a_4)$ and then one with sides $a_1, a_2, |a_3 - a_4|$. One gets two values for θ_2 from each of these, for a total of four, in agreement with the bilinear analysis.

For the four-bar with particular values $\{a_1, a_2, a_3, a_4\} = \{1, 0.6, 0.88, 0.63\}$ and $\theta_1 = 0.$, there are two real solutions: approximately $(\theta_2, \theta_3) = (\pm 0.6970, \mp 2.8837)$. These are shown as red dots on the motion curve in Fig. 3.

3.3 Problem 3: Find all Branches

To draw the complete motion curve, one could solve the forward kinematics (Problem 1) for a finely-sampled set of inputs, x. As this potentially gives many solution points at each x, there remains the task of connecting the points together to form approximations of the branches. Also, to get a uniformly smooth representation of the branches, one needs to sample more densely near the turning points.

A simpler approach is as described in [26] and summarized in [27] which give an algorithm for finding the real points in a complex curve. Essentially, the method is as follows:

1. Find all real turning points (see Problem 2 above) and sort them in ascending input values.
2. Let $t_1 < t_2 < \cdots < t_m$ be the input values at the turning points from Step 1. If there are no turning points, set $t_1 = 0$.
3. For one input value $x_1 < t_1$ and one value x_j, $j = 2, \ldots, m$ in each interval $t_{j-1} < x_j < t_j$, solve the forward kinematics (See Problem 1 above).

4. Trace the mechanism motion arcs from each real solution from Step 3 to its neighboring turning points. As we assume the input is an angle, this means that solutions at x_1 also trace backwards around to t_m.
5. (Optional) Merge together any arcs from Step 4 that meet at a regular point, i.e., not at a turning point.

At the end of this process, we have a list of the branches and a numerical sampling of points along each branch. For the purpose of merely plotting the motion curve, we may skip the final merging step, but then any one branch may be filled in by several of its arcs. The merging step is necessary if we want to determine exactly the number of branches and the full extent of each.

There are several ways to trace the motion arcs as required in Step 4. As software for solving ordinary differential equations (ODEs) is readily available, it can be convenient to convert (14) to the differential equation

$$f_x + f_y(dy/dx) = 0. \tag{22}$$

Step 3 provides the initial conditions for (x,y) and the neighboring turning points provide the ending value of x. An alternative is to use a prediction-correction path-tracking method [24]. In essence, these intersperse ODE methods for advancing along the path (prediction) with the Newton-Raphson method

$$dy = -[f_y]^{-1} f(p,x,y), \qquad y \leftarrow y + dy, \tag{23}$$

at the current value of x. The Newton-Raphson procedure is the correction phase of the prediction-correction cycle, serving to eliminate any accumulation of integration error from the prediction phase.

Note that in Step 2, the absence of any turning points means that either there are no branches at all (the mechanism cannot be assembled) or the input is a crank for all the branches. We replace the empty set of turning values with $t_1 = 0$ so that the next step is cued to discover if any branches exist.

3.4 Problem 4: Find Critical Points

In Problems 1–3, the design parameter p was always given. Now we wish to consider how the behavior of the mechanism changes as the design parameter varies. Consequently, we consider that with p varying, the system (16) becomes $N+1$ variables in $N+2$ unknowns and defines a curve, say $\mathcal{K} \subset \mathbb{C}^{N+2}$, $\dim(\mathcal{K}) = 1$. Since this consists of the turning points as p varies, we call $\mathcal{K}$ the *turning curve*.

To trace out the turning curve as p varies, we wish to carry out the corresponding algorithm as Steps 1–5 played in Problem 3, where we described how to completely describe a motion curve. The analogous process will divide $\mathcal{K}$ into branches, each of which continues monotonically with parameter p. We call the turning points with respect to p of the turning curve simply the *critical points*.

The importance of the critical points is that they mark values of the design parameter where the number of branches in the motion curve can change. Murray [21] describes the resulting mechanism at the critical points as "transition linkages." As the design parameter varies, a pair of branches may disappear where two real turning points meet then become complex, or vice versa, two complex turning points can meet and become real to create a pairs of new branches. While this is the typical behavior, other phenomena are also possible. A singular critical point (for example, a double root of the critical point conditions) might be isolated in the reals and correspond to a degeneracy that exists just at one parameter value. (For example, the motion curve might pinch to touch itself at one value of p and immediately separate on either side.) Another possibility is that the turning curve might cross itself, with some kind of degeneracy occurring at the crossing point.

To find the critical points, we proceed analogously to Problem 1, replacing x by p, y by (x,y), and f by F. The tangency condition (14) becomes

$$\frac{\partial F}{\partial p}\Delta p + \frac{\partial F}{\partial x}\Delta x + \frac{\partial F}{\partial y}\Delta y = 0. \tag{24}$$

Defining $F_{xy} = \begin{bmatrix} \frac{\partial F}{\partial x} & \frac{\partial F}{\partial y} \end{bmatrix}$, the condition for the critical points, analogous to (16), is

$$\begin{bmatrix} F \\ \det F_{xy} \end{bmatrix} = \begin{bmatrix} f \\ \det f_y \\ \det F_{xy} \end{bmatrix} = 0. \tag{25}$$

It is useful to note that

$$F_{xy} = \begin{bmatrix} f_x & f_y \\ \frac{\partial \det f_y}{\partial x} & \frac{\partial \det f_y}{\partial y} \end{bmatrix}. \tag{26}$$

As with turning points, an alternative formulation that avoids forming the determinants is to solve for a tangent vectors that have no x-component and tangent vectors that have no x-component or y-component. That is, randomly choose a $1 \times N$ vectors v and w and solve the system

$$\hat{F}(p,x,y,\Delta x,\Delta y) = \begin{bmatrix} f(p,x,y) \\ f_y \Delta y \\ v \cdot \Delta y - 1 \\ F_{xy}\,[\Delta x\ \Delta y]^T \\ w \cdot [\Delta x\ \Delta y]^T - 1 \end{bmatrix} = 0. \tag{27}$$

Again, as in the case of (17), one must check for the possible existence of solutions where the Jacobian matrices f_y and F_{xy} lose extra rank so that the associated tangent spaces are higher-dimensional.

As in the preceding problems, we use the four-bar to illustrate. To form (16), we already found

$$F = \begin{bmatrix} f \\ D \end{bmatrix}$$

with $f = \{h_2, h_3, H_4\}$ and $D := \det(\frac{\partial H_4}{\partial \theta_3}) = \mathbf{T}_3\overline{\mathbf{R}}_4 - \overline{\mathbf{T}}_3\mathbf{R}_4$. Since the derivatives of h_2 and h_3 are identically zero, see (18), the required derivatives are

$$F_{xy} = \begin{bmatrix} \frac{\partial H_4}{\partial \theta_2} & \frac{\partial H_4}{\partial \theta_3} \\ \frac{\partial D}{\partial \theta_2} & \frac{\partial D}{\partial \theta_3} \end{bmatrix} = \begin{bmatrix} \frac{\partial H_4}{\partial \theta_2} & D \\ \frac{\partial D}{\partial \theta_2} & \frac{\partial D}{\partial \theta_3} \end{bmatrix}. \tag{28}$$

Since $D = 0$ at the critical points, only the diagonal elements contribute to $\det F_{xy}$:

$$\det F_{xy} = \frac{\partial H_4}{\partial \theta_2} \cdot \frac{\partial D}{\partial \theta_3}. \tag{29}$$

The first factor,

$$\frac{\partial H_4}{\partial \theta_2} = i a_2 (T_2\overline{\mathbf{R}}_4 - \mathbf{R}_4\overline{\mathbf{T}}_2), \tag{30}$$

implies that links 2 and 4 are parallel, and since the turning points happen where links 3 and 4 are parallel, we have critical points wherever the linkage folds flat, all in one line. To check the formulation, we solved the system $\{f, D, \frac{\partial H_4}{\partial \theta_2}\} = 0$ using polynomial continuation as implemented in the Bertini software package [25]. Since a_4 only appears as a_4^2, we replaced it by a new variable, say $z = a_4^2$. Then, with variable groups $\{\mathbf{T}_2, \mathbf{T}_3\}, \{\overline{\mathbf{T}}_2, \overline{\mathbf{T}}_3\}, \{z\}$, a three-homogeneous homotopy had six paths. As expected, four of these lead to the solutions:

$$\begin{aligned} a_4^2 &= (a_1 + a_2 + a_3)^2; \\ a_4^2 &= (a_1 + a_2 - a_3)^2; \\ a_4^2 &= (a_1 - a_2 + a_3)^2; \\ a_4^2 &= (-a_1 + a_2 + a_3)^2, \end{aligned} \tag{31}$$

which are consistent with the four-bar transition linkage formulations of [21]. The remaining two solutions gave $a_4 = 0$ with the two possible ways for the dyad of links 2 and 3 to reach the pivot where link 4 attaches to ground. Using $\mathbf{T}_3\overline{\mathbf{T}}_3 = 1$ and (5), the second factor may be written as

$$\frac{\partial D}{\partial \theta_3} = i(\mathbf{T}_3\overline{\mathbf{R}}_4 + \overline{\mathbf{T}}_3\mathbf{R}_4 - 2a_3). \tag{32}$$

The solution of $\{f, D, \frac{\partial H_4}{\partial \theta_3}\} = 0$ using Bertini again used six homotopy paths, but in this case, all paths went to infinity. As the example is a general one, this implies that this system is incompatible and will never give critical points for any set of $\{a_1, a_2, a_3\}$. This is in agreement with existing knowledge about four-bars, where the conditions (31) are known to mark the transitions between mechanisms with different branch numbers.

3.5 Problem 5: Trace out the turning curve

This problem is analogous to Problem 3.3, except this time we wish to trace out the turning curve $\mathcal{K}$ instead of one of the motion curves $\mathcal{C}_p$. Fortunately, we already have in place all the pieces required. In following the five step process of Section 3.3, the adjustments are:

1. Find the critical points (Problem 4).
2. Sort by parameter value p.
3. Solve for turning points (Problem 2) at regular test values of p between the critical ones.
4. Track paths of the turning points using the turning point system $F = 0$ to the neighboring critical values of p.
5. Skip the merge step.

In addition, in Step 3, we find the branches of the motion curve $\mathcal{C}_p$ at each of the regular test values of p (Problem 3). This tells us the character of all the mechanisms in the corresponding interval between the critical points. In particular, the number of branches is constant in each interval.

3.6 Problem 6: Describe the design surface

The collection of motion curves $\mathcal{C}_p$ as we vary p fit together to form a surface. We call it the "design surface," because it shows every motion that can be obtained by varying the design parameter.

An algorithm for numerically describing real polynomial surfaces is given in [27]. In fact, the development of the motion curve, turning points, turning curve, and critical points shown above follows closely the method presented there. The final step to topologically describing the design surface is to find how each branch of the motion curve at a regular parameter value connects to one or more branches in the motion curve for the neighboring critical parameter values.

The issue here is analogous to the curve case where a forward kinematics solution method can be used to roughly approximate a curve by sampling many points on it. The analysis of

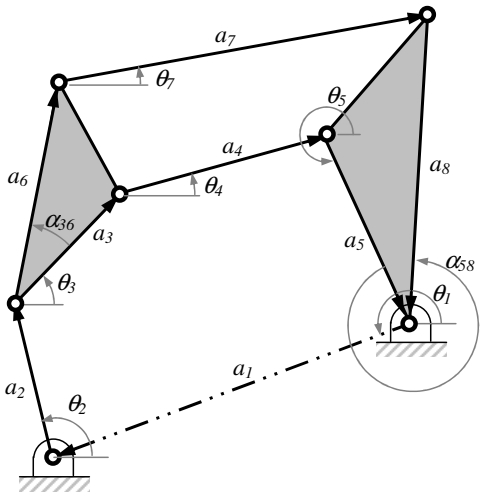

Figure 5: Stephenson II linkage position vector loop.

turning points improves the situation by allowing one to directly trace out each of the branches and join them up properly. In analogy, the curve algorithm allows one to generate a slice of the design surface at various sample values of p. The algorithm of [27] allows one to carve up the surface into two-dimensional cells (analogous to branches of a curve) and connect them properly to form the surface.

For design purposes, it seems good enough to generate slices of the design surface at sample values of p. The critical points tell us where to slice to observe motions with different numbers of branches. Accordingly, we do not pursue a full development of the design surface here. By comparing our developments so far to the corresponding steps in [27], the astute reader can see how to adapt that method to complete the description of the design surface.

4 Example: Stephenson II Linkage

In the initial presentation of our methods, we used the four-bar linkage as an illustration. We now conduct the same procedures for a more substantial example, the Stephenson II linkage shown in Fig. 5. For this exercise, we select $x = \theta_2$ as the input angle and designate the design parameter as $p = a_2$. For the examples in this section, following values are used: $a_1 = 1.00$, $a_3 = 0.60$, $a_4 = 0.90$, $a_5 = 0.70$, $a_6 = 1.00$, $a_7 = 2.0$, $a_8 = 1.50$, $\theta_1 = \pi$, $\alpha_{36} = 0.927$, and $\alpha_{58} = 5.878$. Referring to Figure 5, the position loop equations and the isotropic unit length equations are written as

$$g_1 := a_1\mathbf{T}_1 + a_2\mathbf{T}_2 + a_3\mathbf{T}_3 + a_4\mathbf{T}_4 + a_5\mathbf{T}_5 = 0 \quad (33)$$
$$g_2 := a_1\mathbf{T}_1 + a_2\mathbf{T}_2 + b_6\mathbf{T}_3 + a_7\mathbf{T}_7 + b_8\mathbf{T}_5 = 0 \quad (34)$$
$$\bar{g}_1 := a_1\overline{\mathbf{T}}_1 + a_2\overline{\mathbf{T}}_2 + a_3\overline{\mathbf{T}}_3 + a_4\overline{\mathbf{T}}_4 + a_5\overline{\mathbf{T}}_5 = 0 \quad (35)$$
$$\bar{g}_2 := a_1\overline{\mathbf{T}}_1 + a_2\overline{\mathbf{T}}_2 + b'_6\overline{\mathbf{T}}_3 + a_7\overline{\mathbf{T}}_7 + b'_8\overline{\mathbf{T}}_5 = 0 \quad (36)$$
$$h_j := \mathbf{T}_j\overline{\mathbf{T}}_j - 1 = 0, \qquad j = 2,3,4,5,7 \quad (37)$$

All of the a_j are real link lengths, but b_6 and b_8 are a complex stretch rotation to properly model the ternary link. That is, $b_6 = a_6(\cos\alpha_{36} + i\sin\alpha_{36})$, and likewise for $b_8 = a_8(\cos\alpha_{58} + i\sin\alpha_{58})$. In $\bar{g}_2$, b'_6 and b'_8 are the complex conjugates of b_6 and b_8. Note that $\mathbf{T}_1, \overline{\mathbf{T}}_1$, model the ground link and are known.

As in our treatment of the four-bar, it is advantageous to use the loop equations to eliminate some variables. To this end, two variables per loop are eliminated by defining,

$$\begin{aligned}
\mathbf{R}_4 &:= -(a_1\mathbf{T}_1 + a_2\mathbf{T}_2 + a_3\mathbf{T}_3 + a_5\mathbf{T}_5),\\
\overline{\mathbf{R}}_4 &:= -(a_1\overline{\mathbf{T}}_1 + a_2\overline{\mathbf{T}}_2 + a_3\overline{\mathbf{T}}_3 + a_5\overline{\mathbf{T}}_5),\\
\mathbf{R}_7 &:= -(a_1\mathbf{T}_1 + a_2\mathbf{T}_2 + b_6\mathbf{T}_3 + b_8\mathbf{T}_5),\\
\overline{\mathbf{R}}_7 &:= -(a_1\overline{\mathbf{T}}_1 + a_2\overline{\mathbf{T}}_2 + b'_6\overline{\mathbf{T}}_3 + b'_8\overline{\mathbf{T}}_5),
\end{aligned} \quad (38)$$

with use of which the closure conditions become

$$h_2 = \mathbf{T}_2\overline{\mathbf{T}}_2 - 1 = 0, \quad (39)$$
$$h_3 = \mathbf{T}_3\overline{\mathbf{T}}_3 - 1 = 0, \quad (40)$$
$$H_4 = \mathbf{R}_4\overline{\mathbf{R}}_4 - a_4^2 = 0, \quad (41)$$
$$h_5 = \mathbf{T}_5\overline{\mathbf{T}}_5 - 1 = 0, \quad (42)$$
$$H_7 = \mathbf{R}_7\overline{\mathbf{R}}_7 - a_7^2 = 0. \quad (43)$$

For a given design, the solution of this system of five equations in the six unknowns $\{\mathbf{T}_2, \mathbf{T}_3, \mathbf{T}_5, \overline{\mathbf{T}}_2, \overline{\mathbf{T}}_3, \overline{\mathbf{T}}_5\}$ is the motion curve of the linkage. "Real" solutions are those for which $|\mathbf{T}_2| = |\mathbf{T}_4| = |\mathbf{T}_5| = 1$. At any point on the curve, we can backsolve for the remaining angles using

$$\mathbf{T}_4 = \mathbf{R}_4/a_4, \quad \mathbf{T}_7 = \mathbf{R}_7/a_7. \quad (44)$$

Starting with the loop closure conditions (Eqs. 39-43), we are prepared to do a full analysis of the linkage, including its turning curve and critical points.

4.1 Forward Kinematics

For forward kinematics, the input angle θ_2 is given, and therefore $\mathbf{T}_2$ and $\overline{\mathbf{T}}_2$ are known. The forward kinematics solutions are the roots of Eqs. 40-43, a system of four bilinear equations. The two-homogeneous root count is the coefficient of $\alpha^2\beta^2$

in $(\alpha+\beta)^4$, which is six. Indeed, with θ_2 locked, one sees that the remaining links form a pentad structure, which is known to have at most six assembly configurations [28]. The system can be reduced to a single sextic equation in one variable using the method of [3] or solved as is using polynomial continuation and a six-path homotopy.

4.2 Turning Points

As detailed in Subsection 3.2, the turning points are given by a system of equations consisting of the loop closure conditions (39–43) along with one additional condition $D = 0$, where

$$\begin{aligned} D := \ & \det \begin{bmatrix} \frac{\partial H_4}{\partial \theta_3} & \frac{\partial H_4}{\partial \theta_5} \\ \frac{\partial H_7}{\partial \theta_3} & \frac{\partial H_7}{\partial \theta_5} \end{bmatrix} \qquad (45) \\ = \ & -a3\left[a_4(\mathbf{T}_3\overline{\mathbf{R}}_4 - \mathbf{R}_4\overline{\mathbf{T}}_3)(b_8\mathbf{T}_5\overline{\mathbf{R}}_7 - b'_8\mathbf{R}_7\overline{\mathbf{T}}_5)\right. \\ & \left. -a_5(\mathbf{T}_5\overline{\mathbf{R}}_4 - \mathbf{R}_5\overline{\mathbf{T}}_4)(b_6\mathbf{T}_3\overline{\mathbf{R}}_7 - b'_6\mathbf{R}_7\overline{\mathbf{T}}_3)\right] = 0. \end{aligned}$$

As a two-homogeneous system in the variable groups $\{\mathbf{T}_2, \mathbf{T}_4, \mathbf{T}_5\}, \{\overline{\mathbf{T}}_2, \overline{\mathbf{T}}_4, \overline{\mathbf{T}}_5\}$, the number of roots of the system (39–43,45) cannot be greater than the coefficient of $\alpha^3\beta^3$ in $(\alpha+\beta)^5(2\alpha+2\beta)$, which is $2\binom{6}{3} = 40$. Solving the system using Bertini [25], we find that a general example has at most 24 turning points. For the running example at $a_2 = 0.6$, ten of twenty-four turning points are real. The trace of the turning point curve with a_2 being variable is shown in Fig. 6. As identified in [18], the turning point curve separates the plane into zones with the same number of GIs. Solving the forward kinematic problem for one sample point within each zone determines the number in GIs in the zone, as indicated in Fig. 6

4.3 Critical Points

For the critical points, a_2 remains variable. The system to solve consists of (39–43,45) with one additional equation: $E = \det(\mathcal{E}) = 0$, where

$$\mathcal{E} := \begin{bmatrix} \frac{\partial H_4}{\partial \theta_2} & \frac{\partial H_4}{\partial \theta_3} & \frac{\partial H_4}{\partial \theta_5} \\ \frac{\partial H_7}{\partial \theta_2} & \frac{\partial H_7}{\partial \theta_3} & \frac{\partial H_7}{\partial \theta_5} \\ \frac{\partial D}{\partial \theta_2} & \frac{\partial D}{\partial \theta_3} & \frac{\partial D}{\partial \theta_5} \end{bmatrix}. \qquad (46)$$

However, (46) is very complicated and its determinant is difficult to calculate. Using the alternative formulation from (27), critical points were computed from $\{h_2, H_3, h_4, h_5, H_7\} = 0$ along with $\mathcal{E}\,[\Delta\theta_2\,\Delta\theta_3\,\Delta\theta_4]^T = 0$ and $w \cdot [\Delta\theta_2\,\Delta\theta_3\,\Delta\theta_4]^T = 0$ with a randomly selected w. Using Bertini to solve, critical points exist with a_2 at: 0.1043, 0.1327, 0.2050, 0.3620, 0.4212, 0.6569, 1.3431, 1.7950, 1.8673, 1.8957, 2.3620, 2.4212. These points are identified as local extrema in Fig. 6 and represent the transition

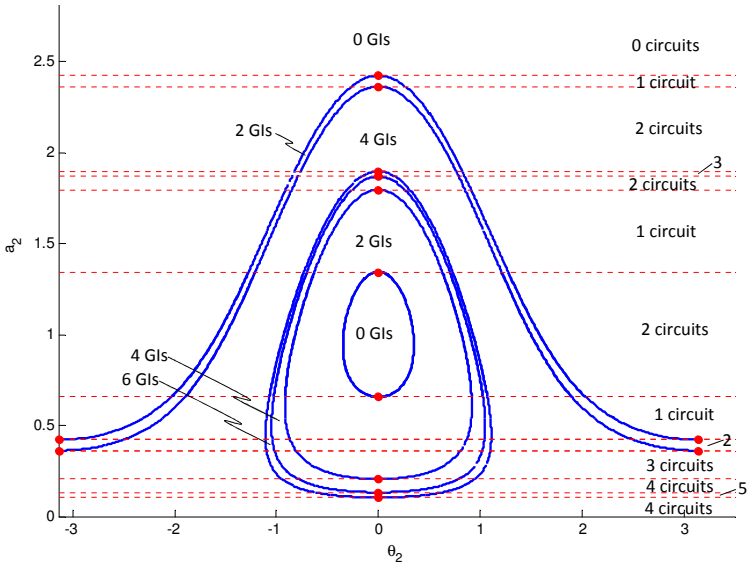

Figure 6: Projection of the Stephenson II turning point curve. Red dots mark the critical points. Regions of equal GIs and circuits are identified.

linkages (bounds of linkages with the same number of circuits). Sampling the motion curve between critical points determines the number of circuits as indicated in Fig. 6.

5 Stephenson III Linkage

In Myszka et. al. [18], a turning point curve was constructed for the the Stephenson III mechanism (originally presented by Chase et. al. [7]) and shown in Fig. 7. For this case, $x = \theta_2$ is the input angle and design parameter is $p = a_7$. The physical parameters values are: $a_1 = 5.1$, $a_2 = 2.93$, $a_3 = 4.3012$, $a_4 = 6.3738$, $a_5 = 8.0623$, $a_6 = 12.0$, $a_7 = 9.5$, $a_8 = 6.0208$, $\theta_1 = \pi/2$, $\theta_6 = 0$, and $\alpha_{48} = 0.529$.

5.1 Loop closure equations

Using isotropic coordinates, the position loop equations and the isotropic unit length equations as

$$g_1 := a_1\mathbf{T}_1 + a_2\mathbf{T}_2 + a_3\mathbf{T}_3 + a_4\mathbf{T}_4 + a_5\mathbf{T}_5 = 0 \qquad (47)$$
$$g_2 := b_4\mathbf{T}_4 + a_5\mathbf{T}_5 + a_6\mathbf{T}_6 + a_7\mathbf{T}_7 = 0 \qquad (48)$$
$$\bar{g}_1 := a_1\overline{\mathbf{T}}_1 + a_2\overline{\mathbf{T}}_2 + a_3\overline{\mathbf{T}}_3 + a_4\overline{\mathbf{T}}_4 + a_5\overline{\mathbf{T}}_5 = 0 \qquad (49)$$
$$\bar{g}_2 := b'_4\overline{\mathbf{T}}_4 + a_5\overline{\mathbf{T}}_5 + a_6\overline{\mathbf{T}}_6 + a_7\overline{\mathbf{T}}_7 = 0 \qquad (50)$$
$$h_j := \mathbf{T}_j\overline{\mathbf{T}}_j - 1 = 0, \qquad j = 2,3,4,5,7 \qquad (51)$$

As before, all of the a_j are real link lengths, but b_4 is a complex stretch rotation to properly model the ternary link. In this case,

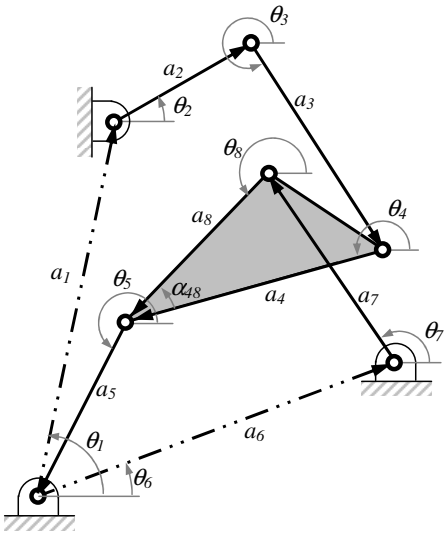

Figure 7: Stephenson III linkage position vector loop.

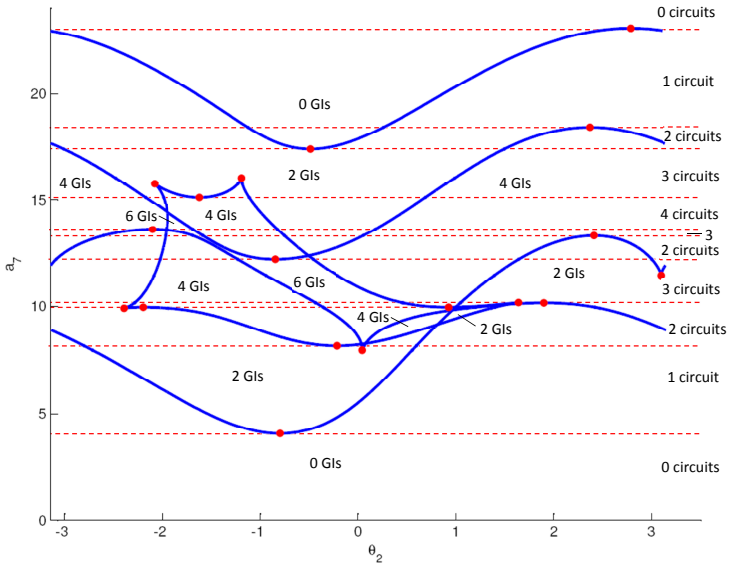

Figure 8: Projection of the Stephenson III turning point curve. Red dots mark the critical points. Regions of equal GIs and circuits are identified.

$\mathbf{T}_1, \mathbf{T}_6, \overline{\mathbf{T}}_1, \overline{\mathbf{T}}_6$ model the ground link and are known. Also, the following definitions will eliminate variables,

$$\begin{aligned}
\mathbf{R}_3 &:= -(a_1\mathbf{T}_1 + a_2\mathbf{T}_2 + a_4\mathbf{T}_4 + a_5\mathbf{T}_5),\\
\overline{\mathbf{R}}_3 &:= -(a_1\overline{\mathbf{T}}_1 + a_2\overline{\mathbf{T}}_2 + a_4\overline{\mathbf{T}}_4 + a_5\overline{\mathbf{T}}_5),\\
\mathbf{R}_7 &:= -(b_4\mathbf{T}_4 + a_5\mathbf{T}_5 + a_6\mathbf{T}_6),\\
\overline{\mathbf{R}}_7 &:= -(b'_4\overline{\mathbf{T}}_4 + a_5\overline{\mathbf{T}}_5 + a_6\overline{\mathbf{T}}_6),
\end{aligned} \tag{52}$$

Using (52), the closure conditions become

$$h_2 = \mathbf{T}_2\overline{\mathbf{T}}_2 - 1 = 0, \tag{53}$$
$$H_3 = \mathbf{R}_3\overline{\mathbf{R}}_3 - a_3^2 = 0, \tag{54}$$
$$h_4 = \mathbf{T}_4\overline{\mathbf{T}}_4 - 1 = 0, \tag{55}$$
$$h_5 = \mathbf{T}_5\overline{\mathbf{T}}_5 - 1 = 0, \tag{56}$$
$$H_7 = \mathbf{R}_7\overline{\mathbf{R}}_7 - a_7^2 = 0. \tag{57}$$

For a given design, the solution of this system of five equations in the six unknowns $\{\mathbf{T}_2, \mathbf{T}_4, \mathbf{T}_5, \overline{\mathbf{T}}_2, \overline{\mathbf{T}}_4, \overline{\mathbf{T}}_5\}$ is the motion curve of the linkage.

Starting with the loop closure conditions (53–57), a full analysis of the Stephenson III linkage, including its turning curve and critical points, proceeds identical to the prior case. For turning points,

$$\begin{aligned}
D :=\ & \det\begin{bmatrix} \frac{\partial H_3}{\partial\theta_4} & \frac{\partial H_3}{\partial\theta_5} \\ \frac{\partial H_7}{\partial\theta_4} & \frac{\partial H_7}{\partial\theta_5} \end{bmatrix} \\
=\ & -a5\left[a_4(\mathbf{T}_4\overline{\mathbf{R}}_3 - \mathbf{R}_3\overline{\mathbf{T}}_4)(\mathbf{T}_5\overline{\mathbf{R}}_7 - \mathbf{R}_7\overline{\mathbf{T}}_5)\right. \\
& \left.-(b_4\mathbf{T}_4\overline{\mathbf{R}}_7 - b'_4\mathbf{R}_7\overline{\mathbf{T}}_4)(\mathbf{T}_5\overline{\mathbf{R}}_3 - \mathbf{R}_3\overline{\mathbf{T}}_5)\right] = 0.
\end{aligned} \tag{58}$$

The trace of the turning point curve with a_7 as a variable is shown in Fig. 8. Solving the forward kinematic problem for one sample point within each zone determines the number of GIs in the zone, as indicated in Fig. 8

For the critical points, a_7 is variable. The system to solve consists of (53–57,58) with one additional equation:

$$E := det\begin{bmatrix} \frac{\partial H_3}{\partial\theta_2} & \frac{\partial H_3}{\partial\theta_4} & \frac{\partial H_3}{\partial\theta_5} \\ 0 & \frac{\partial H_7}{\partial\theta_4} & \frac{\partial H_7}{\partial\theta_5} \\ \frac{\partial D}{\partial\theta_2} & \frac{\partial D}{\partial\theta_3} & \frac{\partial D}{\partial\theta_5} \end{bmatrix} = 0. \tag{59}$$

One may notice that a_7 only appears in H_7, so in fact, we can drop that equation from the system and solve just (53–56,58,59) for $\{\mathbf{T}_2, \mathbf{T}_4, \mathbf{T}_5, \overline{\mathbf{T}}_2, \overline{\mathbf{T}}_4, \overline{\mathbf{T}}_5\}$ and then evaluate a_7 from (57).

Whichever way we choose to treat a_7, it is advantageous to first simplify (59). Expanding the determinant along the first

column, we have

$$E = (\frac{\partial H_3}{\partial \theta_2}) \det \begin{bmatrix} \frac{\partial H_7}{\partial \theta_4} & \frac{\partial H_7}{\partial \theta_5} \\ \frac{\partial D}{\partial \theta_4} & \frac{\partial D}{\partial \theta_5} \end{bmatrix} + (\frac{\partial D}{\partial \theta_2}) D. \tag{60}$$

But $D = 0$, so the second term can be dropped. Thus, E factors as

$$E = E_1 E_2 = (\frac{\partial H_3}{\partial \theta_2}) \det \begin{bmatrix} \frac{\partial H_7}{\partial \theta_4} & \frac{\partial H_7}{\partial \theta_5} \\ \frac{\partial D}{\partial \theta_4} & \frac{\partial D}{\partial \theta_5} \end{bmatrix}. \tag{61}$$

This means we can subdivide the computation of critical points into two separate systems: $\{h_2, H_3, h_4, h_5, H_7, D, E_1\} = 0$ and $\{h_2, H_3, h_4, h_5, H_7, D, E_2\} = 0$.

In the first of these two systems, we have

$$E_1 = \frac{\partial H_3}{\partial \theta_2} = i a_2 (\mathbf{T}_2 \overline{\mathbf{R}}_3 - \mathbf{R}_3 \overline{\mathbf{T}}_2). \tag{62}$$

By Lemma 2.1, we know that this means that links 2 and 3 are parallel. Solving the subsystem with Bertini, we find that it has in general 24 roots. For the particular case at hand, ten of these are real. As in the case of turning points, the lines of links 3, 5, and 7 are concurrent.

To evaluate E_2, we need the partial derivatives $\partial D/\partial \theta_4$ and $\partial D/\partial \theta_5$. This is not as daunting as it might seem, for if we write

$$D = \det \begin{bmatrix} D_{11} & D_{12} \\ D_{21} & D_{22} \end{bmatrix},$$

then by the multilinearity of the determinant, we have

$$\frac{\partial D}{\partial \theta_4} = \det \begin{bmatrix} \frac{\partial D_{11}}{\partial \theta_4} & D_{12} \\ \frac{\partial D_{21}}{\partial \theta_4} & D_{22} \end{bmatrix} + \det \begin{bmatrix} D_{11} & \frac{\partial D_{12}}{\partial \theta_4} \\ D_{21} & \frac{\partial D_{22}}{\partial \theta_4} \end{bmatrix}. \tag{63}$$

and similarly for $\frac{\partial D}{\partial \theta_5}$.

It is not instructive to present all the details. Suffice it to say that E_2 turns out to be degree 6 and the number of paths in a three-homogeneous homotopy with variable groups $\{\mathbf{T}_2, \mathbf{T}_4, \mathbf{T}_5\}, \{\overline{\mathbf{T}}_2, \overline{\mathbf{T}}_4, \overline{\mathbf{T}}_5\}, \{z\}$ is 120. For a general system, Bertini finds that the system has 72 roots, and for the example problem, eight of these are real. Two of the real solutions have the four-bar formed by links 5, 6, 7, and 8 folded collinearly. These have the same length of a_7 and the same four-bar configuration but with the dyad of links 2 and 3 taking two different poses. The other six real solutions are of more general form.

Table 1: Solutions to $\{h_2, H_3, h_4, h_5, H_7, D, E_1\} = 0$ and $\{h_2, H_3, h_4, h_5, H_7, D, E_2\} = 0$.

with $E_1 = 0$	
a_7	θ_2
4.0683	-0.7959
8.1607	-0.2151
10.1662	1.8993
12.2149	-0.8452
13.3276	2.4115
13.6264	-2.0994
15.1138	-1.6217
17.3987	-0.4853
18.4214	2.3714
23.0749	2.7883

with $E_2 = 0$	
a_7	θ_2
8.0363	0.0481
9.9135	-2.3910
9.9585	0.9266
9.9585	-2.1953
10.1802	1.6393
11.4582	3.0987
15.6533	-2.0410
15.9300	-1.2010

A breakdown of all complex solutions to $E_2 = 0$ goes as follows. First, there are four critical points with $a_7 = 0$: two solutions of the triangle formed by links 5, 6, and 8 for each of which there are two solutions of the dyad formed by links 2 and 3. (None of these are real in the example under study.) Second, analogous to the formulas in (31), there are four folded four-bar solutions, each of which gives two solutions for the link 2-3 dyad, for a total of eight. (Only two of these are real in the example.) This leaves $72 - 4 - 8 = 60$ critical points of more general form (of which only six are real in the example). For Stephenson III mechanisms having different values for the remaining linkage parameters, the number of real solutions in each category may change, but for general examples, the counts of 4, 8, and 60 for the complex critical points of each type will remain fixed.

All $10 + 8 = 18$ real solutions are given in Table 1, and these are marked as red dots in Figure 8. Sampling the motion curve between critical points, the number of circuits were determined and indicated on the figure. Notice that the six general-type solutions of $E_2 = 0$ are cusps in the figure.

6 Fully Rotating, Non-Cranking Input Links

In Myszka et. al. [18], ranges of a_7 were identified on the Stephenson III turning point curve that produced a linkage with greater than a fully rotating, non cranking input link. That is, the input link was able to travel greater than 360° between singularities. This occurs when the trace of a branch on the motion

curve with fully rotatable crank folds over itself. On the turning point curve, this characteristic is associated when a change in the design parameter changes the number of singularities but does not change the number of circuits. This happens at critical points that form a cusp on the turning point curve. However, all cusps are not associated with this unique quality, as the fold may not occur on a continuously rotating crank. Yet, it is observed that linkages with greater than 360°, non-rotatable crank are bounded by a cusp. For the Stephenson III explored in Section 5, linkages with a greater than 360°, non-rotatable crank exist for $10.1662 \leq a_7 \leq 11.4582$ and $15.6533 \leq a_7 \leq 15.9300$. Referring back to Fig. 8, these regions are bounded by critical points that appear as cusps.

7 Conclusions

This paper presented a general method to compute the turning curve critical points of single-degree-of-freedom, closed-loop linkages with a designated input angle and one design parameter. For a fixed value of the design parameter, a linkage has turning points, which break the motion curve into branches such that the motion along each branch can be driven monotonically from the input. As the design parameter changes, the turning points sweep out a turning curve and the critical points are the singularities in this curve with respect to the design parameter. Critical points were shown to be associated with transition linkages. The number of branches and their connections may change at certain critical points. The method was illustrated on a four-bar linkage and a Stephenson II linkage. Additionally, the Stephenson III linkage was revisited where the input angle is able to rotate more than one revolution between singularities.

REFERENCES

[1] Erdman, A. Sandor, G. and Kota, S., 2001, *Mechanism Design: Analysis and Synthesis*, Vol. 1, 4/e, Prentice Hall.

[2] Kovacs, P. and Mommel, G., 1993, On the Tangent-Half-Angle Substitution, *Computational Kinematics*, Angeles, J. (editor), Kluwer Academic Publishers, pp. 27-40.

[3] Wampler, C.W., 2001, Solving the Kinematics of Planar Mechanisms by Dixon Determinant and a Complex-Plane Formulation, *ASME J. Mechanical Design*, Vol. 123, 3382–387.

[4] Wampler, C.W., 1999, Solving the Kinematics of Planar Mechanisms *ASME Journal of Mechanical Design*, Vol. 121, 387-391.

[5] Wampler, C.W., 1996, Isotropic Coordinates, Circularity, and Bezout Numbers: Planar Kinematics from a New Perspective *Proceedings of the ASME Design Technical Conference*, Paper 96-DETC/MECH-1210.

[6] Wampler, C.W., and Sommese, A.J., 2011, Numerical Algebraic Geometry and Algebraic Kinematics, *Acta Numerica*, 469–567.

[7] Chase, T. and Mirth, J., 1993, Circuits and Branches of Single-Degree-of-Freedom Planar Linkages, *ASME Journal of Mechanical Design*, vol. 115, No. 2, pp. 223-230.

[8] Foster, D. and Cipra, R., 1998, Assembly Configurations and Branches of Planar Single-Input Dyadic Mechanisms, *ASME Journal of Mechanical Design*, vol. 120, No. 3, pp. 381-386.

[9] Foster, D. and Cipra, R., 2002, An Automatic Method for Finding the Assembly Configurations of Planar Non-Single-Input Dyadic Mechanisms, *ASME Journal of Mechanical Design*, vol. 124, No. 3, pp. 58-67.

[10] Mirth, J. and Chase, T., 1993, Circuit Analysis of Watt Chain Six-Bar Mechanisms, *ASME Journal of Mechanical Design*, vol. 115, No. 2, pp. 214-222.

[11] Davis, H. Chase, T. and Chase, T., 1994, Circuit Analysis of Stephenson Chain Six-Bar Mechanisms, *Proceedings of the ASME Design Technical Conferences*, DE-Vol. 70, pp. 349-358.

[12] Wantanabe, K. and Katoh, H., 2004, Identification of Motion Domains of Planar Six-Link Mechanisms of the Stephenson-Type, *Mechanism and Machine Theory*, vol. 39, pp. 1081-1099.

[13] Ting, K. L., Dou, X., 1996, Classification and Branch Identification of Stephenson Six-bar Chains, *Mechanism and Machine Theory*, vol. 31, no. 3, pp. 283-295.

[14] Litvin, F. and Tan, J., 1989, Singularities in Motion and Displacement Functions of Constrained Mechanical Systems, *International Journal of Robot Research*, vol. 8, No. 2, pp. 30-43.

[15] Gosselin, C. and Angeles, J., 1990, Singularity Analysis of Closed-Loop Kinematic Chains, *IEEE Transactions on Robotics and Automation*, vol. 6, No. 3, pp. 281-290.

[16] Zhou, H., Cheung E. H. M, 2004, Adjustable Four-Bar Linkages for Multi-Phase Motion Generation, *Mechanism and Machine Theory*, vol. 39, No. 3, pp. 261-279.

[17] Naik, D. P., Amarnath, C., 1989, Synthesis of Adjustable Four Bar Function Generators through Five Bar Loop Closure Equations, *Mechanism and Machine Theory*, vol. 24, No. 6, pp. 523-526.

[18] Myszka, D., Murray, A., Schmiedeler, J., 2010, Using a Singularity Locus to Exhibit the Number of Geometric Inversions, Transitions and Circuits of a Linkage, *Proceedings of the ASME International Design Technical Conferences*, pp. 771-781.

[19] Wenger, P., Chablat, D., Zein, M., 1998, Workspace and Assembly-modes in Fully Parallel Manipulators: A Descriptive Study, *Advances in Robot Kinematics*, Kluwer Academic Publishers, pp. 117-126.

[20] Wenger, P., Chablat, D., Zein, M., 2007, Degeneracy Study of the Forward Kinematics of Planar 3-RPR Parallel Ma-

nipulators *ASME Journal of Mechanical Design*, Vol. 129, No. 12, pp. 1265-1268.

[21] Murray, A., Turner, M., Martin, D., 2008, Synthesizing Single DOF Linkages Via Transition Linkage Identification *ASME Journal of Mechanical Design*, Vol. 130, No. 2, 022301.

[22] Nielsen, J., and Roth, B., 1999, Solving the Input/ Output Problem for Planar Mechanisms, *ASME J. Mech. Design*, Vol. 121, No. 2, 206211.

[23] Sommese, A.J., and Wampler, C.W., 2005, *Numerical Solution of Systems of Polynomials Arising In Engineering And Science*, World Scientific Press, Singapore.

[24] Allgower, E.L., and Georg, K., 1997, Numerical Path Following, In *Handbook of numerical analysis*, Vol. V, 3–207, North-Holland, Amsterdam.

[25] Bates, D.J., Hauenstein, J.D., Sommese, A.J., and Wampler, C.W., Bertini: Software for Numerical Algebraic Geometry, available at http://www.nd.edu/∼sommese/bertini.

[26] Lu, Y., Bates, D.J., Sommese, A.J., and Wampler, C.W., 2007, Finding all Real Points of a Complex Curve, In *Proc. Midwest Algebra, Geometry and Its Interactions Conf.*, Contemporary Mathematics, AMS, Vol. 448, 183–205.

[27] Besana, G.M., Di Rocco, S., Hauenstein, J.D., Sommese, A.J., and Wampler, C.W., 2011, Cell decomposition of almost smooth real algebraic surfaces, preprint.

[28] G. Pennock G., D. Kassner, D., 1992, Kinematic Analysis of a Planar Eight-Bar Linkage: Application to a Platform-Type Robot, *ASME J. Mechanical Design*, Vol. 114, 87–95.